Modification of Caloris ejecta blocks by long-lived mass-wasting: A volatile-driven process?

Jack Wright, Susan J. Conway, Costanza Morino, David A Rothery, Matthew R Balme, Caleb I Fassett

Earth and Planetary Science Letters 549 (2020) 116519

Contents lists available at ScienceDirect

Earth and Planetary Science Letters

www.elsevier.com/locate/epsl

Modification of Caloris ejecta blocks by long-lived mass-wasting: A volatile-driven process?

Jack Wright [a,*], Susan J. Conway [b], Costanza Morino [c], David A. Rothery [a], Matthew R. Balme [a], Caleb I. Fassett [d]

[a] School of Physical Sciences, The Open University, Walton Hall, Milton Keynes, MK7 6AA, UK
[b] CNRS UMR 6112, Laboratoire de Planétologie et Géodynamique, Université de Nantes, France
[c] CNRS UMR 5204, Laboratoire EDYTEM, Université Savoie Mont Blanc, Chambéry, France
[d] NASA Marshall Space Flight Center, Huntsville, AL, USA

ARTICLE INFO

Article history:
Received 31 January 2020
Received in revised form 10 August 2020
Accepted 11 August 2020
Available online 25 August 2020
Editor: W.B. McKinnon

Keywords:
Mercury
Caloris basin
impact ejecta
volatiles
molards

ABSTRACT

The Caloris basin is the largest well-preserved impact basin on Mercury. As such, Caloris ejecta afford us an opportunity to study material from Mercury's deep interior with remote sensing. We have made observations of the geomorphology, colour, distribution, and flank slopes of the circum-Caloris knobs. Our observations suggest that these circum-Caloris knobs are modified ejecta blocks from the Caloris impact. High-resolution MESSENGER images show that knobs are conical and relatively uncratered compared with the surrounding plains, which implies the knobs have undergone resurfacing. We have observed material that has sloughed off knobs superposing impact craters that demonstrably postdate the Caloris impact, which requires some knob modification to have been more recent. We have observed hollows, depressions in Mercury's surface generally believed to have been caused by volatile-loss, on and closely associated with several knobs, which indicates that many knobs contain volatile material and that knob modification could extend into Mercury's recent past. Our measurements show that knob flanks typically have slopes of ~21°, which is steep for a mound of unconsolidated material that was originally emplaced ~3.8 Ga. The conical shape of knobs, their steep slopes, the dearth of superposed craters on knobs, and knob superposition relationships with other landforms suggest that Caloris ejecta blocks of arbitrary original shape were modified into their present shapes by long-lived mass-wasting. Mass-wasting must have dominated over impact gardening, which would have produced domal morphologies only. We suggest that mass-wasting was probably driven by volatile-loss, in a manner analogous to terrestrial landforms called 'molards'. If the circum-Caloris knobs are analogous to molards, then they represent a landform and a process hitherto undocumented on Mercury, with implications for the volatile content of the planet's interior. These knobs therefore are prime targets for BepiColombo, which could search for fresh failures and volatile exposures in the knobs.

1. Introduction

The Caloris basin (~1,550 km in diameter) is the largest well-preserved impact structure on Mercury (Murchie et al., 2008). Hummocky plains called the Odin Formation (Fig. 1a; McCauley et al., 1981) are unevenly distributed around the basin and are generally believed to be exposed remnants of Caloris' impact ejecta (Denevi et al., 2013; Ernst et al., 2015; Fassett et al., 2009). Larger (1–10 km across) conic mounds, distributed around Caloris (Fig. 1b; see also Mancinelli et al., 2016), but most abundantly within the Odin Formation, are also believed to be part of Caloris' ejecta (Ackiss et al., 2015). However, an ejecta interpretation of the knobs is not straightforward because the Odin Formation has a resolvably younger crater size-frequency distribution than the Caloris basin itself, which leaves the possibility that the knobs formed by some process unrelated to the impact, such as volcanism (Fassett et al., 2009).

If the knobs are Caloris ejecta, then their materials were probably exhumed from the lower crust or upper mantle (Ernst et al., 2015; Potter and Head, 2017), in which case they represent a rare opportunity to inspect materials from Mercury's deep subsurface. If the knobs are volcanic constructs, then their shapes contain information about the eruption conditions and physical properties of the magmas that formed them. From this, inferences about the

* Corresponding author.
E-mail address: jack.wright@open.ac.uk (J. Wright).

https://doi.org/10.1016/j.epsl.2020.116519

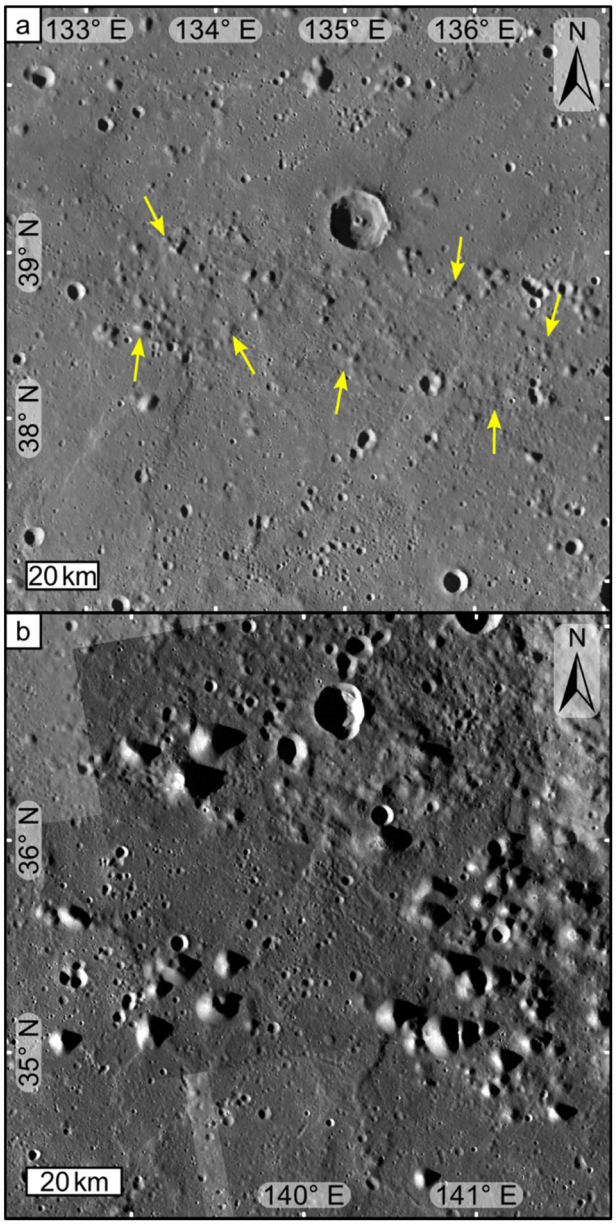

Fig. 1. The Odin Formation and the circum-Caloris knobs. **(a)** The Odin Formation is the knobby material indicated by the yellow arrows. **(b)** Examples of larger circum-Caloris knobs proximal to the Caloris basin rim. EW0220807059G (~86.1 m/pixel), EW0220807071G (~87.7 m/pixel), and EW0220763870G (~88.0 m/pixel). Both panels show the ~166 m/pixel MDIS global monochrome mosaic where individual MDIS frames are not shown. (For interpretation of the colours in the figure, the reader is referred to the web version of this article.)

geophysical and geochemical properties of the melt source region could be made (Sigurdsson et al., 2000). Therefore, it is important that the circum-Caloris knobs be investigated thoroughly.

We used data from NASA's MErcury Surface, Space ENvironment, GEochemistry, and Ranging (MESSENGER) mission to study the distribution, geomorphology, and flank slopes of the circum-Caloris knobs to investigate their origin and evolution.

2. Materials and methods

2.1. Image data

We used the ~166 m/pixel Mercury Dual Imaging System (MDIS; Hawkins et al., 2007) global monochrome mosaic (Chabot et al., 2016) to map the distribution of circum-Caloris knobs > 5 km across using ArcGIS 10.1 software. We implemented this arbitrary size threshold so that our resultant catalogue would be complete. We mapped the circum-Caloris knobs using a Mercator projection centred on the mid-point of Caloris (162.7°E, 31.5°N). We searched for knobs up to 2000 km from the rim of the Caloris basin; a search radius that encapsulated all knobs > 5 km (see supplementary figure S1) across but also allowed us to observe the general distribution of the smallest, most distal knobs. We used MDIS narrow-angle camera (NAC) images with resolutions better than the ~166 m/pixel global mosaic to make geomorphic observations of individual knobs. We also used the ~665 m/pixel enhanced colour mosaic to determine whether the knobs have a distinct colour signature.

2.2. Topographic data

To quantify our geomorphic observations of the circum-Caloris knobs, we plotted topographic profiles of Mercury Laser Altimeter (MLA; Cavanaugh et al., 2007) tracks that sampled close to the summits of mapped knobs.

Few knobs have summit-crossing MLA track data. To measure the topography of knobs lacking MLA data, we used a modified version of the shadow length measurement method of Basilevsky et al. (2002), who developed their method to make topographic profiles of pinnacles on Callisto. In basic shadow length techniques, the trigonometric relationship between the length of the shadow (L) cast in the direction of illumination (Θ) and the incidence angle (i) of the illumination is used to calculate the height (h) of the object casting the shadow. The angle of observation of the shadow, in our case the emission angle (e) of the MESSENGER spacecraft, also affects the calculation (Barnouin et al., 2012). Essentially, h can be calculated by multiplying L by a scaling factor given by:

$$\frac{1}{\tan i \pm \tan e} \tag{1}$$

The method of Basilevsky et al. (2002) applies the scaling factor to the pixels in a spacecraft image. The scaled shadows are then digitised to make topographic profiles of the landforms in the image. Here, we modified the method by instead rotating and scaling digitised outlines of the shadows cast by knobs in map-projected MDIS wide-angle camera (WAC) frames (Fig. 2). This reduced the computational intensity of the method. We used the ET GeoWizards (Tchoukanski, 2017) add-in for ArcGIS to rotate and scale our digitised shadow features. We used WAC frames with a ground resolution of ~100 m/pixel. These are available with suitable shadow measurement lighting geometries for most circum-Caloris knobs. We digitised the shadows of knobs only if they were cast on surfaces that we were confident were both smooth and horizontal. Shadow digitisation was complicated by penumbral shadows, particularly along the 'terminator' shadows on each knob. To make all our digitisations consistent, we always digitised the umbral 'core' of each shadow. Consequently, all knob heights estimated by our method are underestimates, since the shadow lengths from which the heights were calculated were underestimated. All heights are equally affected by this systematic error, which means that overall topographic profile shapes are not distorted.

We measured the characteristic northern and southern flank slopes of each knob using its shadow- and MLA-derived (where available) topographic profile. We calculated slopes by iterative least-squares fitting of first-order polynomials to each topographic profile. We required a minimum of five topographic profile points on each flank to begin the iteration so that flank slope values were not strongly influenced by a small number of points at the edge of each knob. With each iteration, we increased the number of topographic profile points over which each polynomial was

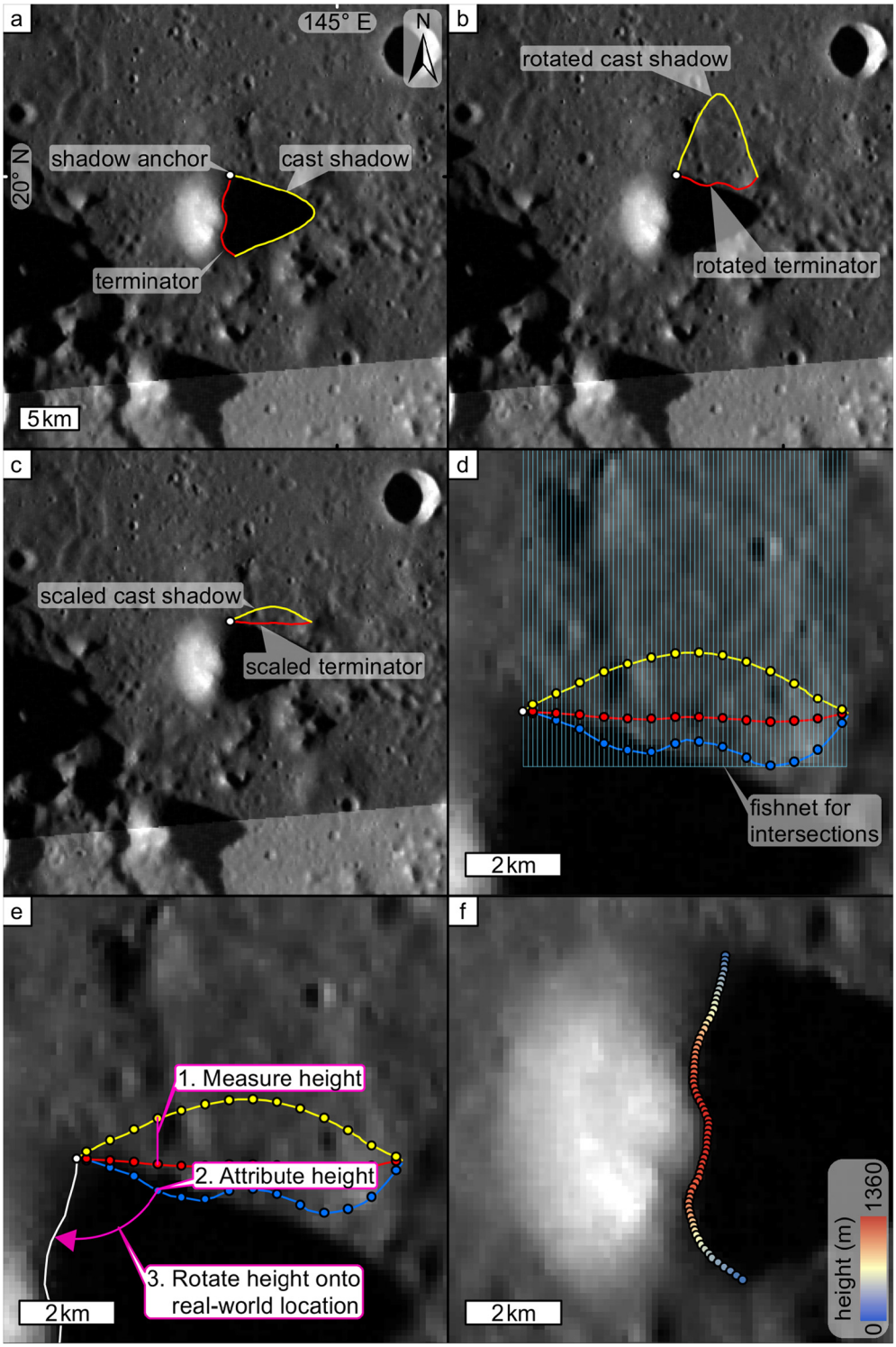

Fig. 2. Method for measuring knob topography from shadows. **(a)** Example of digitised shadow (yellow line) and knob terminator (red line). The shadow anchor (white dot) is the fixed origin for feature rotation and scaling. **(b)** Digitised shadows rotated according to the solar azimuth (Θ) about the shadow anchor so shadows are cast due north. **(c)** Digitised shadows that have been scaled down by a factor calculated using equation (1), relative to the shadow anchor. **(d)** A grid of parallel, north–south lines (a 'fishnet'; light blue), separated by 100 m, is used to link corresponding points on the scaled terminator (red line), scaled cast shadow (yellow line), and rotated, but unscaled terminator (dark blue line). The intersections between the fishnet and the digitisations are marked with appropriately coloured dots. **(e)** In this panel, the distance between a red dot and the yellow dot, measured in the map scale (see scale bar), along their shared fishnet line equals the knob height at the corresponding point on the knob's terminator. This height is attributed to the corresponding blue dot on the rotated, but unscaled terminator. These rotated terminator points with height values are then rotated back onto the knob to place the height data at their true locations. **(f)** A completed shadow-derived knob topographic point dataset (see colour elevation scale). All panels show Mercator projections of EW0220764090G (~125 m/pixel) centred on 162.7°E, 31.5°N. (For interpretation of the colours in the figure, the reader is referred to the web version of this article.)

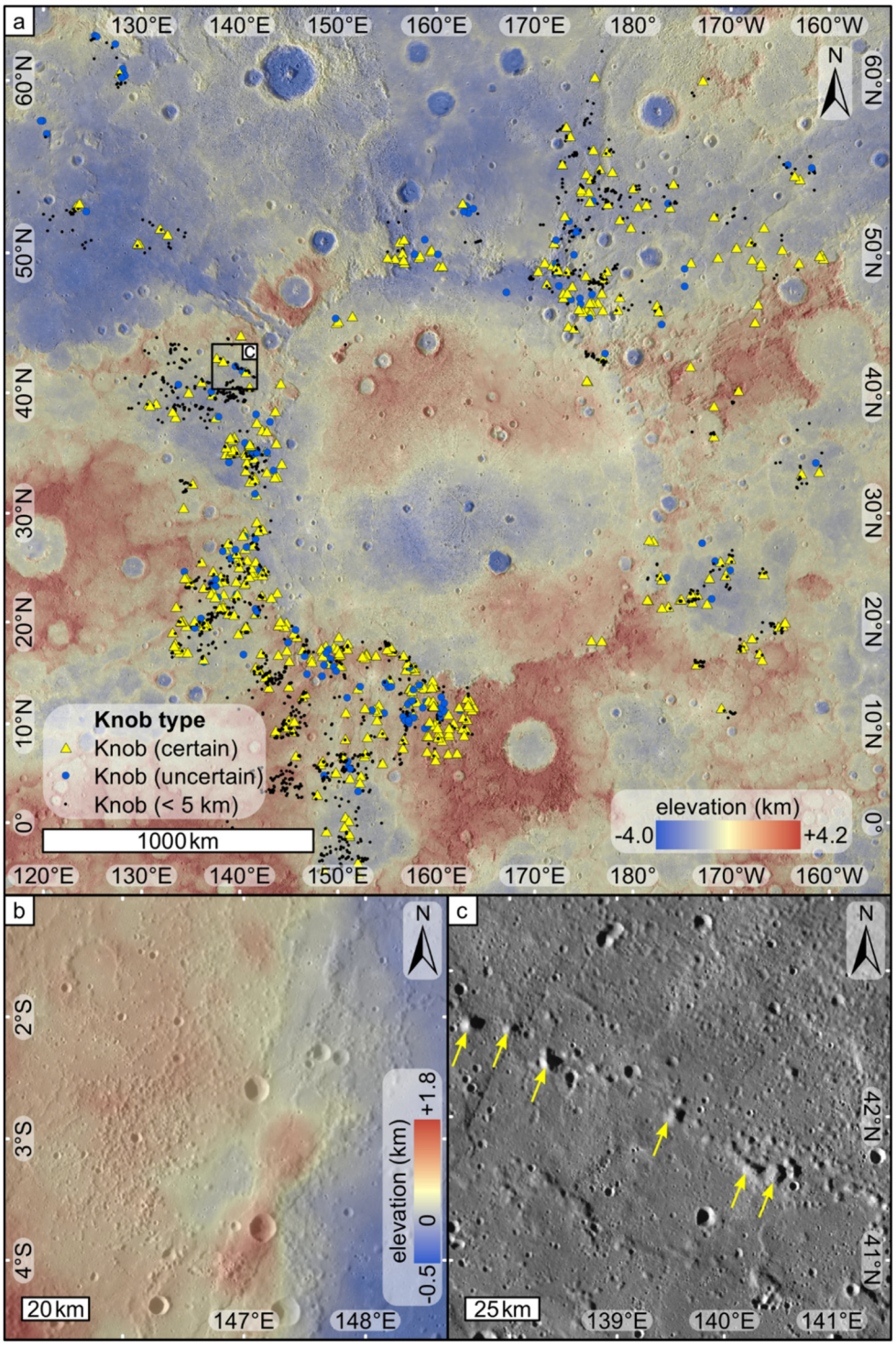

Fig. 3. Distribution of circum-Caloris knobs. **(a)** Knob map shown with the ~665 m/pixel global stereo-digital elevation model (Becker et al., 2016) overlain on the ~166 m/pixel MDIS global monochrome mosaic. Knobs are found at a wide range of absolute elevations. Black box indicates extent of (c). Mercator projection centred on 162.7°E, 31.5°N. **(b)** Topographically controlled contact between knobby (to the west) and smooth plains (to the east). **(c)** Knob chain radial to Caloris (yellow arrows). (For interpretation of the colours in the figure, the reader is referred to the web version of this article.)

fitted by one until the gradient of the determined polynomial began to decrease (usually because the iteration was incorporating profile points from the summit or opposite flank). We took the characteristic flank slope to be the gradient of the steepest polynomial iteration. The northern flank slope was calculated from a topographic profile where the points were arranged from north to south. The points were arranged from south to north for the southern flank slope calculation.

3. Results

3.1. MDIS observations

3.1.1. Knob distribution

We mapped 546 circum-Caloris knobs $\geq$ 5 km across. In Fig. 3a, we show the locations of the circum-Caloris knobs. Knobs are not uniformly distributed around Caloris. They are generally densely

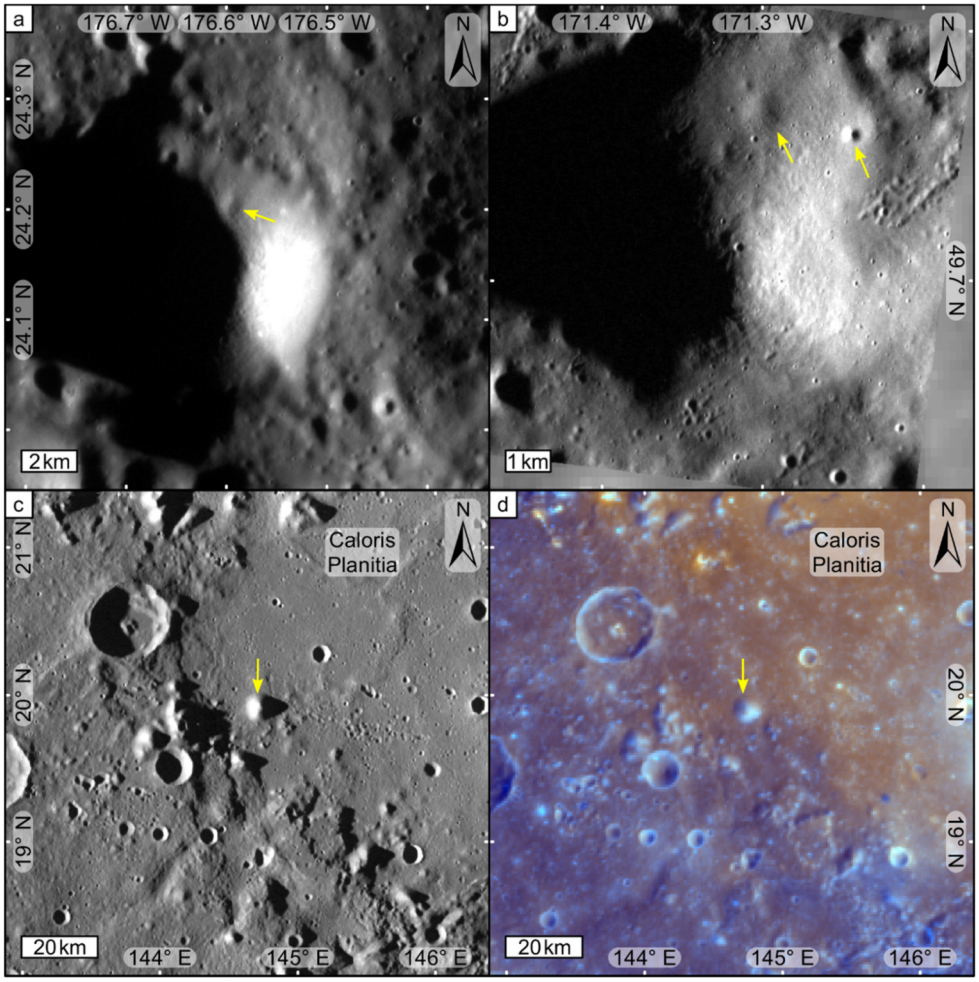

Fig. 4. MDIS observations of knobs. **(a)** A pristine knob. A low, circular depression (yellow arrow) is probably a degraded impact crater. The knob's illuminated flank is otherwise devoid of resolvable craters, indicating efficient resurfacing. EN0258283508M (~37.2 m/pixel). **(b)** A more degraded knob. Small impact craters occur on the knob, but less densely than on the surrounding plains. Larger, degraded craters (yellow arrows) are present. EN1037605314M (~16.2 m/pixel). **(c)** View of the Caloris rim with multiple knobs. Yellow arrow indicates a pristine knob in Caloris Planitia. ~166 m/pixel MDIS global monochrome mosaic. **(d)** Same view as (c) with the ~665 m/pixel MDIS enhanced colour mosaic. Most knobs share the low-reflectance blue colour of the circum-Caloris plains (Denevi et al., 2009). This is most obvious in the case of the knob indicated by the yellow arrow, which contrasts with the high-reflectance red appearance of Caloris Planitia (Denevi et al., 2009). (For interpretation of the colours in the figure, the reader is referred to the web version of this article.)

spaced proximal to the exterior basin rim and more sparsely distributed more distally. The most distal knobs occur ~1,000 km beyond the south-southwestern rim. Knobs are scarce inside the basin, and we found none more than 100 km inside the rim.

As expected, knobs occur most abundantly within the hummocky Odin Formation. Knobs also occur in the smooth plains, however they typically lie close to the smooth plains contact with the Odin Formation. We also observed that much of the Caloris Montes Formation (the uplifted rim of Caloris; Fassett et al., 2009; McCauley et al., 1981) resembles the clusters of knobs seen farther from Caloris' rim.

We observe no relationship between knob density and absolute surface elevation, although this region has long-wavelength topographic undulations (Zuber et al., 2012) that postdate the emplacement of Caloris' smooth plains. However, at local scales knobs occur more abundantly on high-standing topography (Fig. 3b). Locally low-lying regions are more often occupied by smooth plains than by the knobby Odin Formation. We found examples of knobs and knobby plains on the uplifted sides of lobate scarps, and also on the rims of pre-Caloris impact craters; the floors of these craters have been buried by smooth plains.

Knobs are occasionally arranged in chains that radiate approximately from the centre of Caloris (Fig. 3c).

3.1.2. Knob appearance

Isolated circum-Caloris knobs are typically conical to domal in shape (Fig. 4). Knobs commonly occur in overlapping chains and clusters. NAC frames with < 100 m/pixel, available for 75 knobs, show that these landforms are substantially less densely cratered than their surroundings. Most knobs occur within the circum-Caloris plains, which in enhanced colour correspond to low-reflectance blue plains (Denevi et al., 2009). Such knobs usually do not have a strong colour contrast with their surroundings. However, knobs within Caloris Plantia, which corresponds to high-reflectance red plains (Denevi et al., 2009), do have a blue colour contrast with the red plains, which suggests that the knobs are made from different materials to the volcanic plains within Caloris (Fig. 4d; Denevi et al., 2013).

3.1.3. Knobs and other landforms

We have observed 38 knobs that have superposition relationships with impact craters. The basal slopes of some knobs partially obscure impact craters in the surrounding plains (Fig. 5). This means that knob evolution, at least in these examples, far outlasted local plains emplacement, such that these plains could accumulate impact craters that could subsequently be encroached upon by knobs. Blewett et al. (2013) describe a talus apron that probably

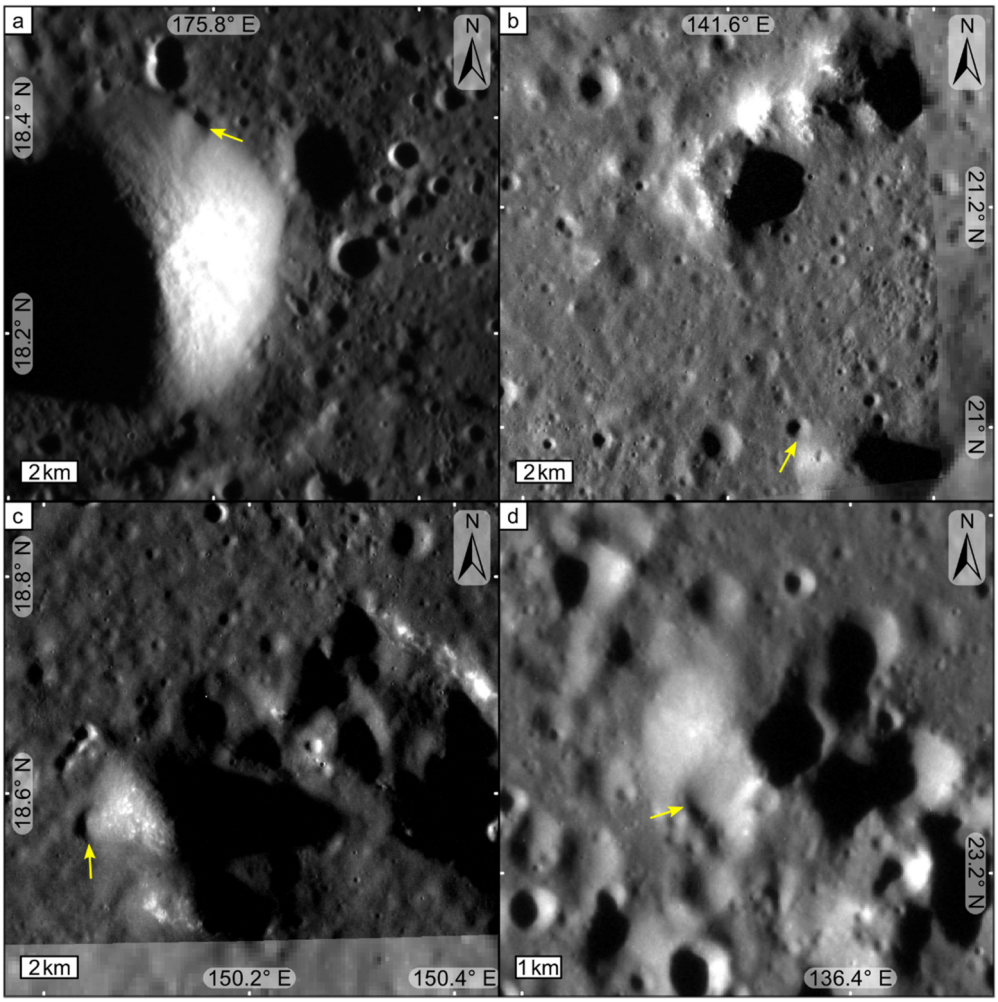

Fig. 5. Knobs partially obscuring impact craters. **(a)** The yellow arrow indicates an impact crater in the smooth plains of Caloris Planitia that is partially obscured by knob material. There is a subtle notch in the knob topographically above this crater, which suggests that knob material cascaded into the crater. EN0258398544M (∼43.2 m/pixel). **(b)** A knob in the lower-right of this panel is partially obscuring an impact crater (yellow arrow) in the Odin Formation. At the top of the panel, two large knobs show evidence of pervasive hollowing. EN0220720878M (∼18.8 m/pixel). **(c,d)** More examples of knobs partially obscuring impact craters (yellow arrows). EN0220764135M (∼19.9 m/pixel) and EN1015541044M (∼39.9 m/pixel), respectively. All panels show MDIS NAC frames overlain on the ∼166 m/pixel MDIS global monochrome mosaic. (For interpretation of the colours in the figure, the reader is referred to the web version of this article.)

formed from mass-wasting of material liberated by hollow formation (discussed later in this section) in the Raditladi basin peak ring. This apron also appears to bury adjacent impact craters and Blewett et al. (2013) suggest this indicates mass-wasting in Raditladi is recent and probably ongoing.

We have found one example of a knob encroaching on a lobate scarp (Fig. 6). The northernmost flanks of this knob appear to be draped over the steep front of the lobate scarp. This lobate scarp cuts across the Caloris rim, which means the most recent movement on this fault postdates the Caloris impact. The majority of the plains cut by this lobate scarp are thought to be volcanic in origin (Denevi et al., 2013; Rothery et al., 2017) and multiple crater size-frequency distribution studies suggest that these plains are ∼100 Myr younger than the Caloris impact (Denevi et al., 2013; Fassett et al., 2009; Mancinelli et al., 2016), although this age difference has been disputed (Ernst et al., 2017). Nevertheless, the knob superposes the lobate scarp, which means that either its formation, or its most recent evolution, must postdate the most recent movement on the scarp. We have observed a back-scarp graben on this lobate scarp. Such grabens are small compared with their host lobate scarps, and thus are more rapidly erased by impact gardening than the main scarp (Watters et al., 2016). The fact that this lobate scarp still has a back-scarp graben in the vicinity of a circum-Caloris knob that abuts the scarp further suggests that the most recent fault movement was geologically recent and consequently that the knob has been modified long after the Caloris impact.

We have observed 10 examples of hollows in close association with knobs (Fig. 7). Hollows are irregular, rimless, steep-sided, flat-floored depressions only a few tens of metres deep (Blewett et al., 2011). They are thought to be caused by the loss of some volatile crustal component to space, which leads to the opening of a cavity that expands laterally by scarp retreat (Blewett et al., 2011). Observations by Vaughan et al. (2012) suggest that hollows form from layers where the lost volatile component constitutes a relatively large proportion of the material in the layer, which explains why hollow floors are generally flat, with only minor bumps that are probable remnants of the inert material left behind from the original surface (Blewett et al., 2011). The absence of observable impact craters on the floors of hollows, in addition to their characteristic bright, optically immature appearance, suggests that they are among the youngest landforms on Mercury and that they might still be forming in the present-day (Blewett et al., 2011). The hollows on the circum-Caloris knobs appear to be forming in original knob materials, rather than material that postdates knob formation, such as subsequent impact ejecta superposing the knobs.

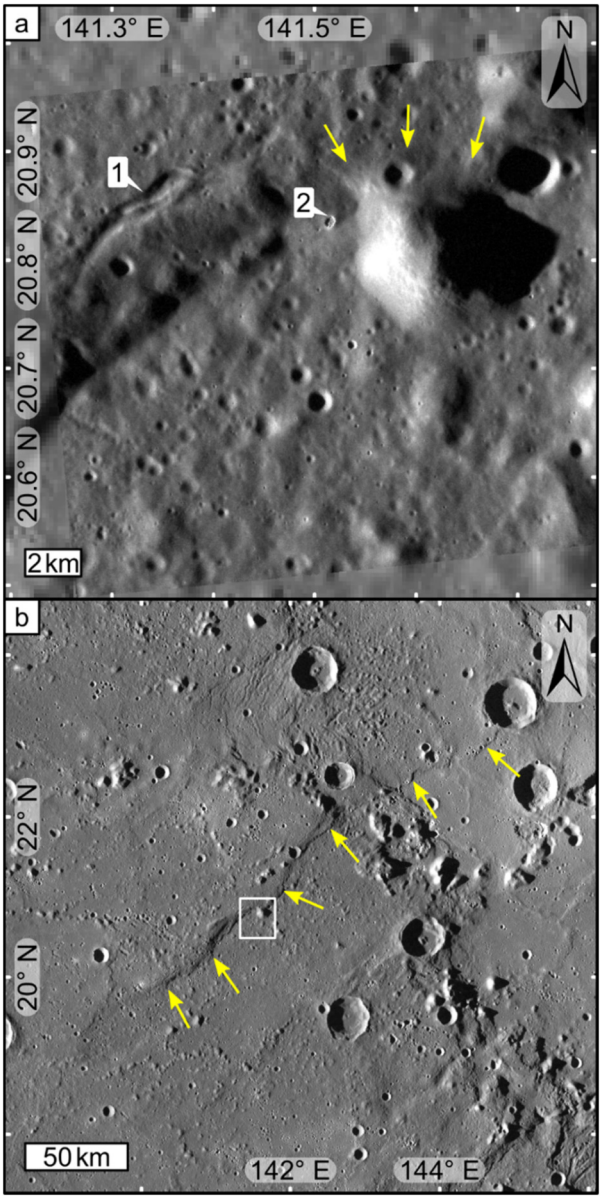

Fig. 6. Knob abutting lobate scarp. **(a)** A knob with flank materials draped over a lobate scarp (yellow arrows). Label 1 indicates a back-scarp graben. Such grabens have been used as evidence for geologically young fault movement on their host lobate scarps elsewhere on Mercury (Watters et al., 2016). A hollow (label 2) has formed in the Odin Formation hosting the knob. NAC frame EN0220720885M (~19.1 m/pixel). **(b)** This lobate scarp (yellow arrows) cuts the circum-Caloris plains, the Caloris rim, and Caloris Planitia, which requires fault movement after the Caloris impact. White box indicates extent of (a). ~166 m/pixel global MDIS monochrome mosaic. (For interpretation of the colours in the figure, the reader is referred to the web version of this article.)

Knobs with pervasive hollowing are always domal (Fig. 7b, c, d). Conical knobs can have hollows, but they are always small compared with the size of the knob (Fig. 7a).

3.2. Knob topography

Of the 545 knobs ≥ 5 km across, 22 had MLA tracks with useful data. These data show that pristine circum-Caloris knobs typically have planar flank slopes, whereas any knobs that are scarred by impact craters are more likely to have convex-up flanks. Flank slopes calculated from MLA data range between ~6–25° (median 18.5°), however both the lower and upper limits of this range will be underestimates since most MLA tracks do not traverse knobs along the lines of steepest ascent and descent. Knobs > 10 km across are rare, but MLA measured heights of ~2 km for two such knobs.

134 circum-Caloris knobs cast shadows that were suitable for digitisation. Of these, 15 had MLA data for comparison. For a straightforward comparison of MLA- and shadow-derived topographic profiles to be made, the traverses of a given knob by the MLA and shadow profiles must closely coincide, which was the case in four examples only. Where MLA- and shadow-derived profiles approximately coincide, the shapes and calculated slopes of the profiles match very well (Fig. 8).

Fig. 9a shows a histogram of flank slopes for the circum-Caloris knobs measured from their shadow-derived topographies. Knob slopes peak between 20° and 25° (median ~21°). There is no difference between northern and southern slopes. Some terrestrial and lunar examples (discussed in Sections 4.4 and 4.5) are included for comparison.

4. Discussion

4.1. Knob origin

Our MDIS observations of the circum-Caloris knobs lead us to the following interpretations. The knobs are Caloris ejecta, rather than volcanic constructs. While the conical and domal shapes of knobs are generally consistent with volcanic constructs elsewhere in the Solar System, they are inconsistent with observations of volcanic landforms on Mercury (Wright et al., 2018). They lack summit craters, which would be predicted for the highly explosive eruptions that occur on airless bodies. This distinguishes the knobs from the few candidate constructional volcanic edifices elsewhere on Mercury (Wright et al., 2018). Furthermore, the knobs lack the bright red appearance in enhanced colour that is characteristic of explosive volcanism on Mercury (Denevi et al., 2009). Lastly, the occurrence of hollows in knobs appears to be incompatible with the knobs being effusive volcanic constructs; hollows are strongly anti-correlated with Mercury's volcanic smooth plains (Denevi et al., 2013).

In addition, we do not see evidence of knobs forming as outliers from continuous surfaces, or other evidence they are a remnant of a formerly more continuous layer. They appear to be discrete objects in the landscape. Our study therefore affirms the conclusion that the knobs are Caloris ejecta block remnants (Ackiss et al., 2015).

We do not know what the emplacement shapes of these knobs were. If the original blocks had a relatively high strength, then they possibly could retain arbitrary shapes upon deposition. However, it is probable that the kinetic energy dissipated during their deposition was able to overcome their strength, at least partially, such that the blocks disaggregated to some degree into talus with flank slopes up to the angle of repose. Therefore, it is possible that the initial shapes of the knobs were cones or domes. The overlapping knobs shown in Fig. 1b might offer a clue. If the conical shapes of the knobs are primary to their emplacement, then knob clusters would require several ejecta blocks to land in very close proximity. A more parsimonious explanation, given the observations of ejecta block modification (see Section 4.2), is that they formed from one large ejecta block of arbitrary shape that encompassed them all. We must therefore consider that the present-day conical shapes of the knobs are potentially secondary to their formation.

4.2. Ejecta block modification

We have demonstrated for the first time that knobs around Caloris have been modified after their original formation. Modification has been long-lived, as evidenced by knobs that encroach on

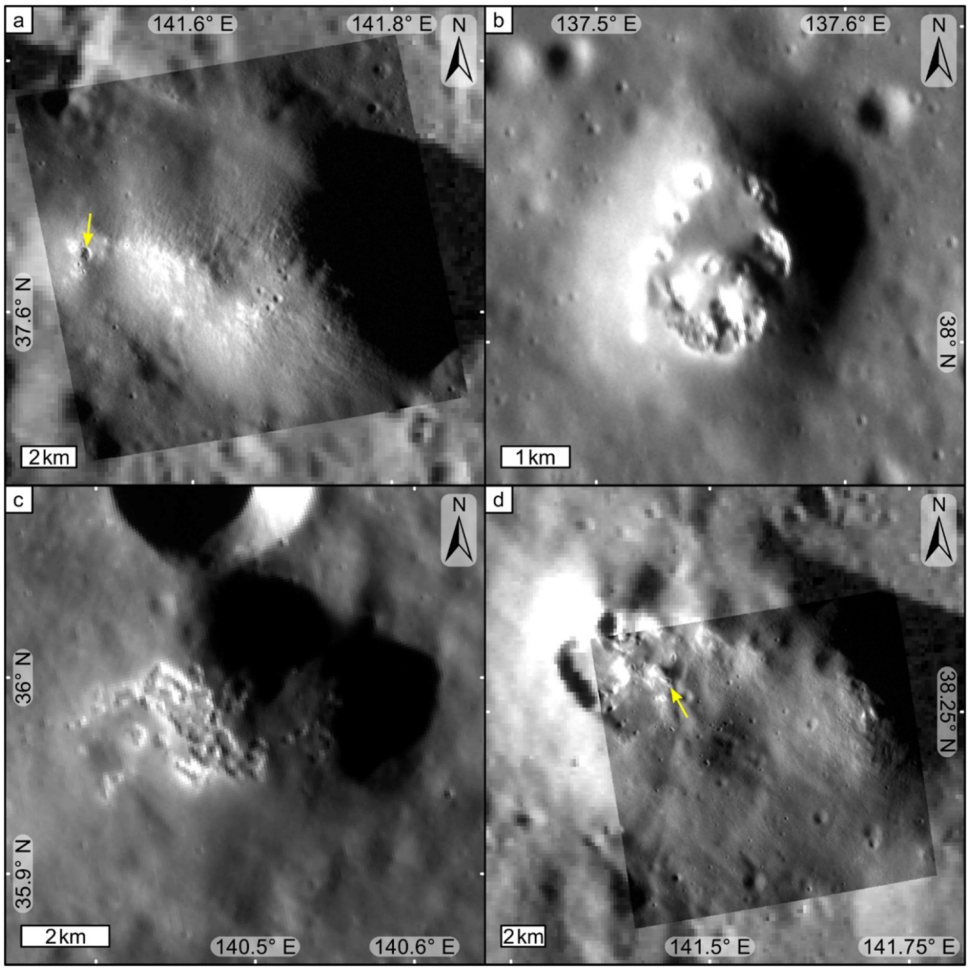

Fig. 7. Knobs and hollows. **(a)** An elongate, pristine knob with resolved surface texture. The yellow arrow indicates a hollow on the flank of the knob. EN0220720623M (~12.4 m/pixel). **(b)** A near-complete ring of hollows encircles a knob's summit. EN1045703448M (~28.8 m/pixel). **(c)** A domal knob with pervasive hollowing. EN1045674576M (~61.2 m/pixel). **(d)** Two overlapping knobs. The western knob is unusual in that Thomas et al. (2014a) identified a volcanic vent in it. The yellow arrow indicates hollows identified by Thomas et al. (2014b). All panels show MDIS NAC frames overlain on the ~166 m/pixel global MDIS monochrome mosaic. (For interpretation of the colours in the figure, the reader is referred to the web version of this article.)

landforms such as impact craters and lobate scarps that necessarily postdate Caloris ejecta emplacement. Furthermore, modification probably has lasted in many cases into the recent past, as evidenced by hollow formation within many knobs. It is probable that modification continues today, as is supposed for hollows (Blewett et al., 2018) and for bright, spectrally blue streaks that have been observed on young (Mansurian or later) steep slopes on Mercury, which have been suggested to be mass-movements triggered by volatile-loss (Malliband et al., 2019).

An ejecta origin for the circum-Caloris knobs requires their materials, presumably ejecta blocks, to have been emplaced at ~3.5–3.8 Ga, when the Caloris basin formed (Denevi et al., 2018). Following emplacement, the ejecta blocks would have undergone erosion and degradation. On Mercury, physical degradation of landforms is chiefly due to the formation of impact craters, which mobilise material target material downslope (Fassett et al., 2017). This impact gardening is a diffusive process that decreases topographic curvature (i.e. sharp topographic contrasts relax over time; Fassett et al., 2017). Therefore, ~3.8 Gyr of impact gardening of Caloris ejecta blocks of any original shape would produce rounded landforms and lower their slopes with time (Fassett and Thomson, 2014).

We have shown multiple examples of knobs with steep conical shapes, but conical shapes are not predicted by erosion of arbitrarily shaped ejecta blocks by diffusive processes. To 'sharpen' an arbitrarily shaped ejecta block into a cone, or maintain the shape of an originally conical knob, an advective mass transport mechanism is required; i.e. one that efficiently transports mass downslope. Furthermore, this mass transport mechanism needs to be faster than erosion caused by impact gardening and long-lived enough for conical knobs to be observable today.

Hollows on Mercury appear to grow laterally by scarp retreat (Blewett et al., 2011), in which volatile-loss causes removal of material from the sides of a depression and exposes fresh surfaces. This in turn allows further volatile-loss from the fresh surface. Inert material would be deposited at the foot of the retreating scarp, but hollows appear to form by the removal of relatively pure volatile layers (Vaughan et al., 2012). Scarp retreat is therefore an advective mass transport mechanism that could be a candidate for the modification of arbitrarily shaped Caloris ejecta blocks into conical knobs. If volatile loss was involved in the formation of the circum-Caloris knobs (section 4.3), then the concentration of volatiles must be lower than in the case of hollows for the slopes of inert material to form.

4.3. Volatile-driven knob evolution

We have shown several examples of knob materials that contain hollows, which suggests that at least some of Caloris' impact ejecta is volatile-rich. Volatile-bearing Caloris ejecta is supported

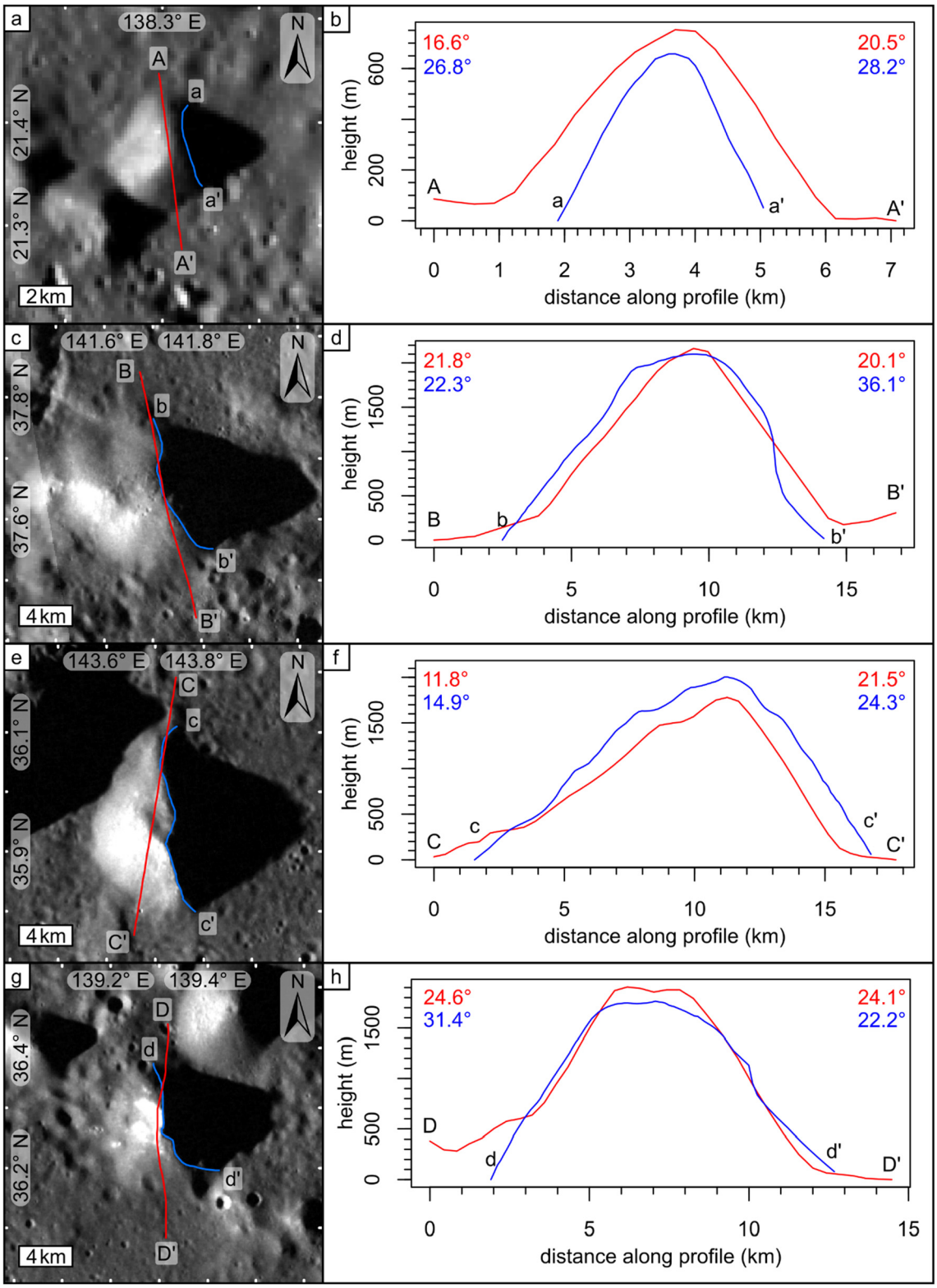

Fig. 8. Comparison of MLA- and shadow-derived topographic profiles of knobs. **(a,c,e,g)** Knobs with their topographic profile traverses. Red = MLA-derived, blue = shadow-derived. EW0220893691G (124 m/pixel), EW0220763834G (83 m/pixel), EW0220763859G (86 m/pixel), and EW0220807059G (86 m/pixel) respectively. **(b,d,f,h)** Knob topographic profiles. Colours and labels correspond with the panels opposite. (For interpretation of the colours in the figure, the reader is referred to the web version of this article.)

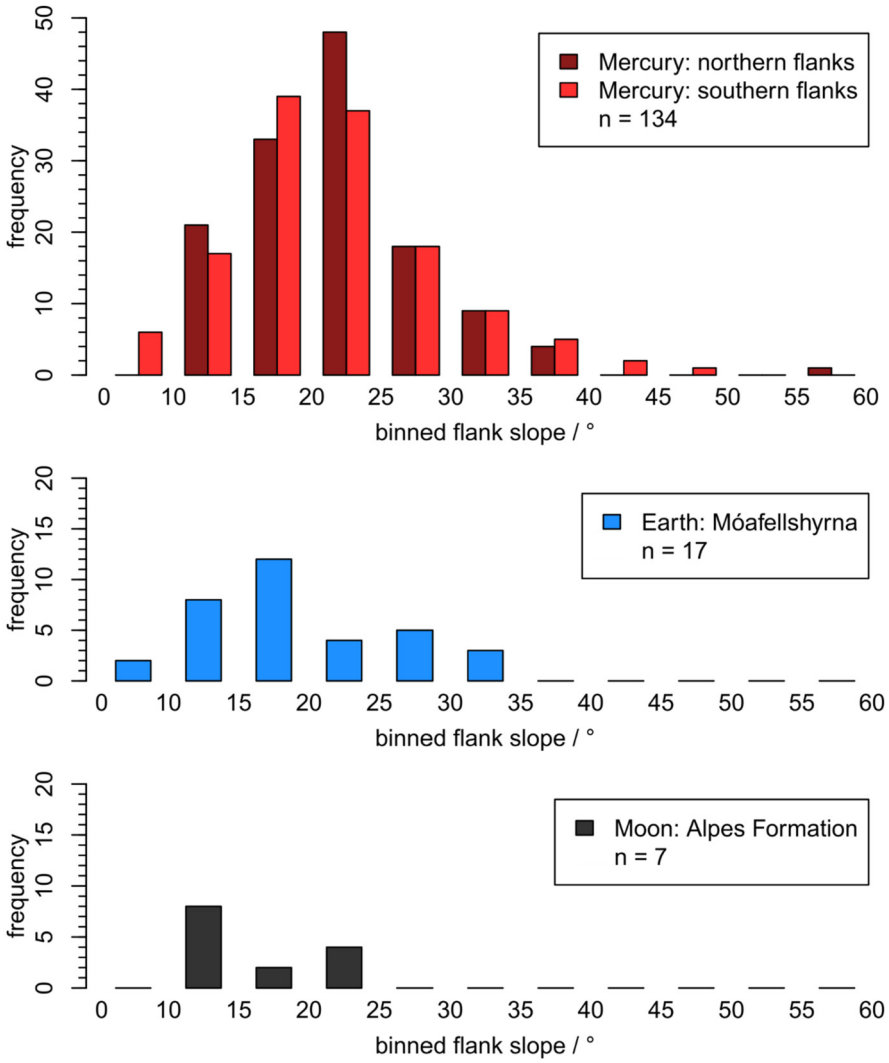

Fig. 9. Comparison of knob slopes. Shadow-derived data for 134 circum-Caloris (Mercury) knobs are plotted (northern and southern flank slopes are separated). LiDAR-derived data for 17 molards from the Móafellshyrna landslide, Earth (Morino et al., 2019). LOLA-derived data for seven Alpes Formation (Moon) knobs that are interpreted as Imbrium ejecta blocks (Wilhelms et al., 1987; Wilhelms and McCauley, 1971).

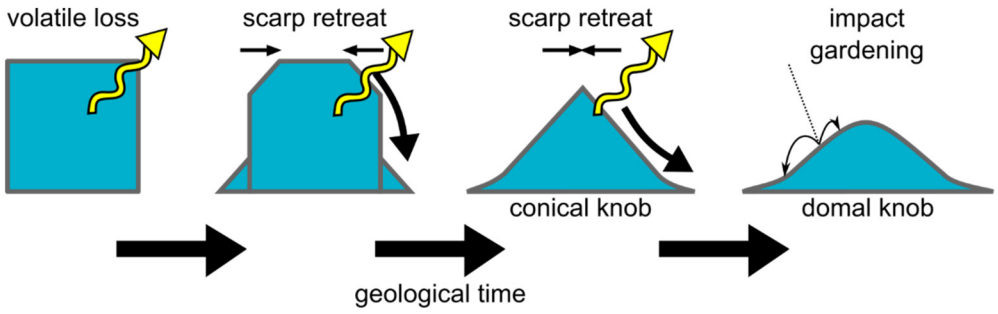

Fig. 10. Concept of knob evolution. An ejecta block with an arbitrary starting shape contains a structurally integral volatile component. Volatile material is lost to space and the remaining inert material disintegrates and collects at the foot of the block as a debris pile. More volatile material is exposed, which forms the block into a conical knob by scarp retreat. Once scarp retreat becomes slow compared with impact gardening, the knob is modified to be more dome shaped.

by observations of apparently volatile-rich low-reflectance material excavated from beneath Caloris (Ernst et al., 2015). If a structurally integral volatile material is located within a knob, then devolatilisation of this component could cause downslope movement of the disaggregated, non-volatile component (Fig. 10). The pile of unconsolidated material at the base of the block would build up planar slopes to the angle of repose (~32°; Barnouin et al., 2012) before becoming oversteepened. If the slopes became oversteepened then they would fail as a gravity flow or slump and cause material to spread outward from the developing knob.

As long as there was exposed volatile material, the ejecta block would have continued to degrade by devolatilisation, which would form a conical knob or cluster of knobs. Continued devolatilisation would maintain knobs in conical forms as long as impact gardening was outpaced by mass-wasting.

Exhaustion of the volatile component, or entombment of the volatile source by a sufficiently thick lag deposit, would cause scarp retreat to cease. At this stage of knob evolution, impact gardening would have dominated and caused steep, conical knobs to be modified into lower, domal knobs.

Although some Caloris ejecta appears to have been volatile-rich, this does not necessitate volatile involvement in the evolution of Caloris ejecta blocks. However, we have made several observations that support a rapid (for Mercury's surface), advective erosional process capable of turning arbitrarily shaped ejecta blocks into the present-day knobs. The dearth of impact craters on knob flanks requires efficient knob surface renewal, particularly since these blocks were emplaced ∼3.8 Ga. Our observations of knob material partially burying impact craters and abutting lobate scarps that postdate ejecta emplacement provide evidence that long-lived and voluminous mass-wasting has occurred during at least some knobs' histories, which supports a resurfacing process just as efficient as hollow formation.

Volatile-driven scarp retreat and mass-wasting appear to have shaped other planetary surfaces in a similar manner to that which we describe here. Pinnacles on Callisto are thought to have formed by sublimation of ice, primarily from impact crater walls, leading to mass-wasting of non-ice material to form debris piles (Moore et al., 1999). Basilevsky et al. (2002) used their shadow-derived topographic profiles to measure flank slopes of 24 pinnacles (range 17–56°, mean 31.4°, standard deviation 7.9°). These slope measurements, close to the angle of repose and generally planar, support the sublimation-driven mass-wasting hypothesis (Basilevsky et al., 2002). The similarity of our topographic observations of the circum-Caloris knobs to the Callisto pinnacles supports our hypothesis of volatile-driven mass-wasting having modified Caloris ejecta.

It is still uncertain what process causes hollow-forming materials to volatilise. Sublimation, thermal desorption, photon-stimulated desorption, solar wind exposure, and micrometeorite sputtering are all plausible mechanisms (Blewett et al., 2018). The circum-Caloris knobs might offer some insight to this problem. Most knobs are located in Mercury's northern hemisphere, which means their northern flanks are pole-facing, and their southern flanks are equator-facing (i.e. Sun-facing). The absence of an obvious preference for steeper, active slopes on Sun-facing slopes might suggest that insolation-driven processes are not dominant over non-insolation-driven processes, such as micrometeorite bombardment. Furthermore, if volatile-loss is thermally-driven, then re-radiated heat from the surroundings of the circum-Caloris knobs might compensate for the asymmetry of direct insolation, as appears to be the case for the sublimation of Callisto's pinnacles (White et al., 2016).

4.4. Molards: an analogous landform?

The volatile-driven knob formation process we have described is conceptually similar to the formation of landforms observed on Earth called 'molards' (Morino et al., 2019). Briefly, molards are cones of debris on landslide deposits (e.g., Cassie et al., 1988; Cruden, 1982). Molards in permafrost terrains form from thawing of blocks of ice-cemented material mobilised by a landslide. The ice-cementing action allows the material to remain integral during transport. After deposition, the ice thaws, leaving the remaining rock and/or soil to collapse into a mound (Morino et al., 2019).

Notwithstanding the size disparity between the circum-Caloris knobs and molards, and the different magnitudes of the forces that created these landforms, the principle of an excavated volatile-rich ejecta block on Mercury is similar to a thawing ice-rich block on Earth. The observation of molards at different stages of their development (i.e. blocks, cones, and domes) raises the possibility that a similar process could have formed the circum-Caloris knobs, which exhibit conical and domal varieties.

In Fig. 9, we show the flank slope data for the molards from the Móafellshyrna landslide, Iceland, Earth (Morino et al., 2019). These molards are interpreted to have formed from rockfalls, where competent, ice-cemented blocks of sediment detach, fall, and are deposited as discrete entities (Morino et al., 2019). We consider rockfall to be the most analogous molard emplacement mechanism to ejecta block deposition on Mercury because they create discrete landforms. Móafellshyrna molards have a similar slope-frequency distribution to the circum-Caloris knobs (e.g., the frequency peak at ∼20°). In addition, the maximum Móafellshyrna flank slope value is 31.4° (i.e., close to the angle of repose; ∼32°), which is indicative of molard evolution being driven by mass-wasting. The same trend toward the angle of repose is observed in the circum-Caloris knob data, if the four slope measurements $> 40°$ are regarded as outliers (e.g. due to shadow digitisation errors). These similarities support the hypothesis that molards, being landforms that evolve by volatile-loss, are analogous to the circum-Caloris knobs.

A further similarity between molards and the circum-Caloris knobs is the apparent effect of their volatile content on their morphology. Conical molards formed from rockfall blocks that were 15–20% ice by volume (Sæmundsson et al., 2018). Morino et al. (2019) observed that the higher the initial ground ice content was, the lower the final molard heights and flank slopes, and the more domed the summits were. Morino et al. (2019) suggest that very high ice:debris ratios would make molards deflate similarly to a thawing ice-cored moraine. The circum-Caloris knobs with pervasive hollowing clearly have relatively high volatile contents in their near sub-surface. Such knobs also have lower heights, flank slopes, and domal rather than conical shapes. This suggests that, as with ice-cemented blocks and molards on Earth, there is a relationship between the original volatile content of Caloris ejecta and the resultant knobs' shapes.

4.5. Comparison with the lunar Alpes Formation

To test if circum-Caloris knob evolution is necessarily volatile-loss driven, we employed our methodology to the knobs in the lunar Alpes Formation, which is interpreted as Imbrium basin ejecta (Wilhelms et al., 1987; Wilhelms and McCauley, 1971). Compared with Mercury, the Moon is volatile-poor, but, being an airless body, the surface environments of the two bodies are otherwise similar. Furthermore, Imbrium is of comparable size and age (∼3.9 Ga; Liu et al., 2012; Merle et al., 2014) to Caloris. If volatile-loss was a significant factor in the formation of conical circum-Caloris knobs, then no similar conical ejecta remnants would be expected at Imbrium on the volatile-poor Moon.

We used the gridded Lunar Orbiter Laser Altimeter (LOLA; Smith et al., 2010) digital elevation model to measure topographic profiles of the largest knobs in the Alpes Formation. The Montes Alpes, which resemble larger circum-Caloris knobs, are interpreted as uplifted Imbrium rim elements (Wilhelms et al., 1987; Wilhelms and McCauley, 1971), rather than ejecta blocks.

We found seven knobs $\geq$ 5 km across in the Alpes Formation that are not interpreted as rim elements, but as ejecta blocks instead (Wilhelms et al., 1987; Wilhelms and McCauley, 1971). We observed no examples of lunar knobs partially obscuring impact craters. Furthermore, lunar knob slopes are $<23°$ (median $= 14°$), and thus ∼33% lower than the circum-Caloris knob slopes. This evidence suggests mass-wasting has not governed geologically recent Alpes Formation knob evolution, which could indicate that these knobs are not analogous to the circum-Caloris knobs.

4.6. Implications of volatile-rich Caloris ejecta

Objections have been raised about the interpretation of the Odin Formation as Caloris ejecta based on its younger crater size-frequency distribution than other Caloris materials (Denevi et al., 2013). However, if the Odin Formation was emplaced as a volatile-rich ejecta sheet that degraded to produce the knobby appearance that it exhibits today, then it could be possible that its physical properties mean it has unusual crater production/retention properties. This could be a substantial enough effect to give the Odin Formation a younger crater size-frequency distribution relative to the Caloris rim.

We observed many circum-Caloris knobs close within the Caloris rim. It is possible that nearby blocky, isolated massifs of the Caloris Montes Formation formed as a result of scarp retreat and that some such massifs have been modified into clusters of knobs as a result of volatiles having been uplifted into the rim from depth. Widespread devolatilisation and degradation of the Caloris rim might have made it easier for the rim to be inundated by lavas, leading to the smooth plains continuity between Caloris Planitia and the circum-Caloris smooth plains (Rothery et al., 2017).

The most important implication of volatile-rich Caloris ejecta is that the circum-Caloris knobs could provide insight into the composition and material properties of Mercury's interior. On Earth, permafrost degradation appears to produce different shapes of molard landforms depending on the original volume of cementing ice (Morino et al., 2019). If the circum-Caloris knobs formed by devolatilisation of Caloris ejecta blocks, then careful analysis of the shapes of pristine knobs might be used to estimate the volume fraction of the volatile species in the substratum from which the blocks were excavated. Caloris impact modelling predicts the impact's overturned flap would excavate mantle material for a 50 km-thick crust on Mercury (Potter and Head, 2017). Arguments have recently been made that the mean crustal thickness on Mercury might be even thinner, 26 $\pm$ 11 km, which would make widespread mantle excavation by Caloris even more likely (Sori, 2018). Therefore, the circum-Caloris knobs might represent the most easily observed lower crustal or upper mantle material exposed at the surface of Mercury, which makes them important targets for high-resolution remote-sensing by the BepiColombo mission (Benkhoff et al., 2010; Rothery et al., 2020).

5. Conclusions

Our observations of the circum-Caloris knobs argue strongly that they are not small volcanic constructs; an alternative proposed to avoid the problems associated with their interpretation as Caloris ejecta blocks (Fassett et al., 2009). We have made observations that strengthen the hypothesis that the circum-Caloris knobs originated as Caloris ejecta (Ackiss et al., 2015). Observations that support an ejecta origin for the knobs include their non-volcanic colour signature, their lack of volcanic craters, their arrangement in clusters proximal to, and chains radial from, Caloris, and their apparent preservation on locally high-standing topography. The presence of hollows on knobs also argues against a volcanic interpretation of the knobs.

Regardless of how the Caloris ejecta blocks were modified into the circum-Caloris knobs observed today, our observations have made it clear for the first time that this modification process was long-lived, since knob material has been able to spread laterally to obscure small, post-Caloris impact craters and abut lobate scarps that cross-cut Caloris. Our observations refute the hypothesis that the circum-Caloris knobs are volcanic constructs.

Furthermore, our measurements of knob slopes approaching the angle of repose, in conjunction with the association of hollows with knobs, suggest that the circum-Caloris knobs might be analogous to molards on Earth. If this is true, then the circum-Caloris knobs represent a hitherto unrecognised landform on Mercury, formed by an undocumented physical process on that planet, and they provide evidence that Mercury's interior, including at least down to the upper mantle, is volatile-rich. Therefore, these knobs are prime targets for BepiColombo, which could search for fresh failures and volatile exposures in the knobs.

CRediT authorship contribution statement

Jack Wright: Conceptualization, Data curation, Formal analysis, Funding acquisition, Investigation, Methodology, Software, Visualization, Writing - original draft, Writing - review & editing. **Susan J. Conway:** Conceptualization, Formal analysis, Methodology, Resources, Software, Supervision, Validation, Writing - review & editing. **Costanza Morino:** Conceptualization, Investigation, Validation, Writing - original draft, Writing - review & editing. **David A. Rothery:** Conceptualization, Funding acquisition, Project administration, Supervision, Writing - review & editing. **Matthew R. Balme:** Conceptualization, Supervision, Writing - review & editing. **Caleb I. Fassett:** Validation, Writing - review & editing.

Declaration of competing interest

The authors declare no competing interests.

Acknowledgements

The planetary data products used in this work are publicly available from the Planetary Data System (PDS). MESSENGER data are credited to NASA/Johns Hopkins University Applied Physics Laboratory/Carnegie Institute of Washington. The lunar topographic data are credited to the LOLA team. J. Wright was funded by a postgraduate studentship grant (ST/N50421X/1) from the UK Science and Technology Facilities Council (STFC) while collecting and analysing the data for this manuscript. J. Wright acknowledges the financial support from Région Pays de la Loire, project GeoPlaNet, which facilitated in-person collaboration with S.J. Conway and C. Morino in May 2019. J. Wright, D.A. Rothery, and M.R. Balme were funded by PLANMAP during the write-up of this manuscript. PLANMAP has received funding from the European Union's Horizon 2020 research and innovation programme under grant agreement No 776276. J. Wright is also grateful to the Royal Astronomical Society and the Lunar and Planetary Institute for travel awards to present this work at international conferences. J. Wright is grateful to F.E.G. Butcher for helping to develop the ArcGIS workflow that generated the shadow-derived topographic profiles. S.J. Conway was supported for her BepiColombo work by the French Space Agency CNES. C. Morino was supported by a CENTA NERC postgraduate studentship grant (NE/L002493/1), a British Geological Survey BUFI CASE studentship grant (GA/14S/024, Ref: 284), and acknowledges the financial support from Région Pays de la Loire, project GeoPlaNet (convention N° 2016-10982). S.J. Conway and C. Morino were funded by the Agence Nationale de la Recherche in the framework of the project ANR-19-CE01-0010 PERMOLARDS. C.I. Fassett was supported by a NASA Discovery Data Analysis Program grant, Analysis of Large-scale Resurfacing Processes on Mercury. The authors are grateful to the two anonymous reviewers for their encouraging comments and insightful recommendations, which improved the quality of the manuscript. The authors are also grateful to W.B. McKinnon for his editorial handling of the manuscript.

Appendix A. Supplementary material

Supplementary material related to this article can be found online at https://doi.org/10.1016/j.epsl.2020.116519.

References

Ackiss, S.E., Buczkowski, D.L., Ernst, C.M., McBeck, J.A., Seelos, K.D., 2015. Knob heights within circum-Caloris geologic units on Mercury: interpretations of the geologic history of the region. Earth Planet. Sci. Lett. 430, 542–550.

Barnouin, O.S., Zuber, M.T., Smith, D.E., Neumann, G.A., Herrick, R.R., Chappelow, J.E., Murchie, S.L., Prockter, L.M., 2012. The morphology of craters on Mercury: results from MESSENGER flybys. Icarus 219, 414–427.

Basilevsky, A.T., Kryuchkov, V.P., Ivanov, M.A., Zabalueva, E.V., Kotova, I.V., 2002. The morphology of small craters and knobs on the surface of Jupiter's satellite Callisto. Sol. Syst. Res. 36, 322–333.

Becker, K.J., Robinson, M.S., Becker, T.L., Weller, L.A., Edmundson, K.L., Neumann, G.A., Perry, M.E., Solomon, S.C., 2016. First global digital elevation model of Mercury. In: 47th Lunar and Planetary Science Conference. The Woodlands, Houston. Abstract #2959.

Benkhoff, J., van Casteren, J., Hayakawa, H., Fujimoto, M., Laakso, H., Novara, M., Ferri, P., Middleton, H.R., Ziethe, R., 2010. BepiColombo—comprehensive exploration of Mercury: mission overview and science goals. Planet. Space Sci. 58, 2–20.

Blewett, D.T., Chabot, N.L., Denevi, B.W., Ernst, C.M., Head, J.W., Izenberg, N.R., Murchie, S.L., Solomon, S.C., Nittler, L.R., McCoy, T.J., Xiao, Z., Baker, D.M.H., Fassett, C.I., Braden, S.E., Oberst, J., Scholten, F., Preusker, F., Hurwitz, D.M., 2011. Hollows on Mercury: MESSENGER evidence for geologically recent volatile-related activity. Science 80 (333), 1856–1859.

Blewett, D.T., Ernst, C.M., Murchie, S.L., Vilas, F., 2018. Mercury's hollows. In: Solomon, S.C., Nittler, L.R., Anderson, B.J. (Eds.), Mercury: The View After MESSENGER. Cambridge University Press, pp. 324–345.

Blewett, D.T., Vaughan, W.M., Xiao, Z., Chabot, N.L., Denevi, B.W., Ernst, C.M., Helbert, J., D'Amore, M., Maturilli, A., Head, J.W., Solomon, S.C., 2013. Mercury's hollows: constraints on formation and composition from analysis of geological setting and spectral reflectance. J. Geophys. Res., Planets 118, 1013–1032.

Cassie, J.W., Van Gassen, W., Cruden, D.M., 1988. Laboratory analogue of the formation of molards, cones of rock-avalanche debris. Geology 16, 735–738.

Cavanaugh, J.F., Smith, J.C., Sun, X., Bartels, A.E., Ramos-Izquierdo, L., Krebs, D.J., McGarry, J.F., Trunzo, R., Novo-Gradac, A.M., Britt, J.L., Karsh, J., Katz, R.B., Lukemire, A.T., Szymkiewicz, R., Berry, D.L., Swinski, J.P., Neumann, G.A., Zuber, M.T., Smith, D.E., 2007. The Mercury laser altimeter instrument for the MESSENGER mission. Space Sci. Rev. 131, 451–479.

Chabot, N.L., Denevi, B.W., Murchie, S.L., Hash, C.D., Ernst, C.M., Blewett, D.T., Nair, H., Laslo, N.R., Solomon, S.C., 2016. Mapping Mercury: global imaging strategy and products from the MESSENGER mission. In: 47th Lunar and Planetary Science Conference. The Woodlands, Houston, p. 1256.

Cruden, D.M., 1982. The Brazeau Lake slide, Jasper National Park, Alberta. Can. J. Earth Sci. 19, 975–981.

Denevi, B.W., Ernst, C.M., Meyer, H.M., Robinson, M.S., Murchie, S.L., Whitten, J.L., Head, J.W., Watters, T.R., Solomon, S.C., Ostrach, L.R., Chapman, C.R., Byrne, P.K., Klimczak, C., Peplowski, P.N., 2013. The distribution and origin of smooth plains on Mercury. J. Geophys. Res., Planets 118, 891–907.

Denevi, B.W., Ernst, C.M., Prockter, L.M., Robinson, M.S., 2018. The geologic history of Mercury. In: Solomon, S.C., Nittler, L.R., Anderson, B.J. (Eds.), Mercury: The View After MESSENGER. Cambridge University Press, pp. 144–175.

Denevi, B.W., Robinson, M.S., Solomon, S.C., Murchie, S.L., Blewett, D.T., Domingue, D.L., McCoy, T.J., Ernst, C.M., Head, J.W., Watters, T.R., Chabot, N.L., 2009. The evolution of Mercury's crust: a global perspective from MESSENGER. Science 80 (324), 613–618.

Ernst, C.M., Denevi, B.W., Barnouin, O.S., Klimczak, C., Chabot, N.L., Head, J.W., Murchie, S.L., Neumann, G.A., Prockter, L.M., Robinson, M.S., Solomon, S.C., Watters, T.R., 2015. Stratigraphy of the Caloris basin, Mercury: implications for volcanic history and basin impact melt. Icarus 250, 413–429.

Ernst, C.M., Denevi, B.W., Ostrach, L.R., 2017. Updated absolute age estimates for the Tolstoj and Caloris basins, Mercury. In: 48th Lunar and Planetary Science Conference. The Woodlands, Houston. Abstract #2934.

Fassett, C.I., Crowley, M.C., Leight, C., Dyar, M.D., Minton, D.A., Hirabayashi, M., Thomson, B.J., Watters, W.A., 2017. Evidence for rapid topographic evolution and crater degradation on Mercury from simple crater morphometry. Geophys. Res. Lett. 44, 5326–5335.

Fassett, C.I., Head, J.W., Blewett, D.T., Chapman, C.R., Dickson, J.L., Murchie, S.L., Solomon, S.C., Watters, T.R., 2009. Caloris impact basin: exterior geomorphology, stratigraphy, morphometry, radial sculpture, and smooth plains deposits. Earth Planet. Sci. Lett. 285, 297–308.

Fassett, C.I., Thomson, B.J., 2014. Crater degradation on the lunar maria: topographic diffusion and the rate of erosion on the Moon. J. Geophys. Res., Planets 119, 2255–2271.

Hawkins, S.E., Boldt, J.D., Darlington, E.H., Espiritu, R., Gold, R.E., Gotwols, B., Grey, M.P., Hash, C.D., Hayes, J.R., Jaskulek, S.E., Kardian, C.J., Keller, M.R., Malaret, E.R., Murchie, S.L., Murphy, P.K., Peacock, K., Prockter, L.M., Reiter, R.A., Robinson, M.S., Schaefer, E.D., Shelton, R.G., Sterner, R.E., Taylor, H.W., Watters, T.R., Williams, B.D., 2007. The Mercury dual imaging system on the MESSENGER spacecraft. Space Sci. Rev. 131, 247–338.

Liu, D., Jolliff, B.L., Zeigler, R.A., Korotev, R.L., Wan, Y., Xie, H., Zhang, Y., Dong, C., Wang, W., 2012. Comparative zircon U-Pb geochronology of impact melt breccias from Apollo 12 and lunar meteorite SaU 169, and implications for the age of the Imbrium impact. Earth Planet. Sci. Lett. 319–320, 277–286.

Malliband, C.C., Conway, S.J., Rothery, D.A., Balme, M.R., 2019. Potential identification of downslope mass movements on Mercury driven by volatile-loss. In: 50th Lunar and Planetary Science Conference. Abstract #1804.

Mancinelli, P., Minelli, F., Pauselli, C., Federico, C., 2016. Geology of the Raditladi quadrangle, Mercury (H04). J. Maps 5647, 1–13.

McCauley, J.F., Guest, J.E., Schaber, G.G., Trask, N.J., Greeley, R., 1981. Stratigraphy of the Caloris basin, Mercury. Icarus 47, 184–202.

Merle, R.E., Nemchin, A.A., Grange, M.L., Whitehouse, M.J., Pidgeon, R.T., 2014. High resolution U-Pb ages of Ca-phosphates in Apollo 14 breccias: implications for the age of the Imbrium impact. Meteorit. Planet. Sci. 49, 2241–2251.

Moore, J.M., Asphaug, E., Morrison, D., Spencer, J.R., Chapman, C.R., Bierhaus, B., Sullivan, R.J., Chuang, F.C., Klemaszewski, J.E., Greeley, R., Bender, K.C., Geissler, P.E., Helfenstein, P., Pilcher, C.B., 1999. Mass movement and landform degradation on the Icy Galilean satellites: results of the Galileo nominal mission. Icarus 140, 294–312.

Morino, C., Conway, S.J., Sæmundsson, Þ., Helgason, J.K., Hillier, J., Butcher, F.E.G., Balme, M.R., Kneisel, C., Jordan, C., Argles, T., 2019. Molards as an indicator of permafrost degradation and landslide processes. Earth Planet. Sci. Lett. 516, 136–147.

Murchie, S.L., Watters, T.R., Robinson, M.S., Head, J.W., Strom, R.G., Chapman, C.R., Solomon, S.C., McClintock, W.E., Prockter, L.M., Domingue, D.L., Blewett, D.T., 2008. Geology of the Caloris basin, Mercury: a view from MESSENGER. Science 80 (321), 73–76.

Potter, R.W.K., Head, J.W., 2017. Basin formation on Mercury: Caloris and the origin of its low-reflectance material. Earth Planet. Sci. Lett. 474, 427–435.

Rothery, D.A., Mancinelli, P., Guzzetta, L., Wright, J., 2017. Mercury's Caloris basin: continuity between the interior and exterior plains. J. Geophys. Res., Planets 122, 560–576.

Rothery, D.A., Massironi, M., Alemanno, G., Barraud, O., Besse, S., Bott, N., Brunetto, R., Bunce, E., Byrne, P., Capaccioni, F., Capria, M.T., Carli, C., Charlier, B., Cornet, T., Cremonese, G., D'Amore, M., De Sanctis, M.C., Doressoundiram, A., Ferranti, L., Filacchione, G., Galluzzi, V., Giacomini, L., Grande, M., Guzzetta, L.G., Helbert, J., Heyner, D., Hiesinger, H., Hussmann, H., Hyodo, R., Kohout, T., Kozyrev, A., Litvak, M., Lucchetti, A., Malakhov, A., Malliband, C., Mancinelli, P., Martikainen, J., Martindale, A., Maturilli, A., Milillo, A., Mitrofanov, I., Mokrousov, M., Morlok, A., Muinonen, K., Namur, O., Owens, A., Nittler, L.R., Oliveira, J.S., Palumbo, P., Pajola, M., Pegg, D.L., Penttilä, A., Politi, R., Quarati, F., Re, C., Sanin, A., Schulz, R., Stangarone, C., Stojic, A., Tretiyakov, V., Väisänen, T., Varatharajan, I., Weber, I., Wright, J., Wurz, P., Zambon, F., 2020. Rationale for BepiColombo studies of Mercury's surface and composition. Space Sci. Rev. 216, 66.

Sæmundsson, Þ., Morino, C., Helgason, J.K., Conway, S.J., Pétursson, H.G., 2018. The triggering factors of the Móafellshyrna debris slide in northern Iceland: intense precipitation, earthquake activity and thawing of mountain permafrost. Sci. Total Environ. 621, 1163–1175.

Sigurdsson, H., Houghton, B.F., McNutt, S.R., Rymer, H., Stix, J., 2000. The Encyclopedia of Volcanoes, first edn. Academic Press, San Diego, California.

Smith, D.E., Zuber, M.T., Jackson, G.B., Riris, H., Neumann, G.A., Sun, X., McGarry, J.F., Cavanaugh, J.F., Ramos-Izquierdo, L.A., Zellar, R., Torrence, M.H., Mazarico, E., Connelly, J., Matuszeski, A., Ott, M., Rowlands, D.D., Zagwodzki, T., Torrence, M.H., Katz, R., Kleyner, I., Peters, C., Liiva, P., Coltharp, C., Schmidt, S., Ramsey, L., Scott, V.S., Unger, G., Krebs, D.C., Novo-Gradac, A.-M.D., Shaw, G.B., Yu, A.W., 2010. The lunar orbiter laser altimeter investigation on the lunar reconnaissance orbiter mission. Space Sci. Rev. 150, 209–241.

Sori, M.M., 2018. A thin, dense crust for Mercury. Earth Planet. Sci. Lett. 489, 92–99.

Tchoukanski I., ET Geo Wizards, 2017.

Thomas, R.J., Rothery, D.A., Conway, S.J., Anand, M., 2014a. Mechanisms of explosive volcanism on Mercury: implications from its global distribution and morphology. J. Geophys. Res., Planets 119, 2239–2254.

Thomas, R.J., Rothery, D.A., Conway, S.J., Anand, M., 2014b. Hollows on Mercury: materials and mechanisms involved in their formation. Icarus 229, 221–235.

Vaughan, W.M., Helbert, J., Blewett, D.T., Head, J.W., Murchie, S.L., Gwinner, K., McCoy, T.J., Solomon, S.C., 2012. Hollow-forming layers in impact craters on Mercury: massive sulfide or chloride deposits formed by impact melt differentiation? In: 43rd Lunar and Planetary Science Conference. Abstract #1187.

Watters, T.R., Daud, K., Banks, M.E., Selvans, M.M., Chapman, C.R., Ernst, C.M., 2016. Recent tectonic activity on Mercury revealed by small thrust fault scarps. Nat. Geosci. 9, 743–747.

White, O.L., Umurhan, O.M., Moore, J.M., Howard, A.D., 2016. Modeling of ice pinnacle formation on Callisto. J. Geophys. Res., Planets 121, 21–45.

Wilhelms D.E., McCauley J.F., 1971. Geologic map of the near side of the Moon, U.S. Geol. Surv. Misc. Geol. Inv. Map I-703.

Wilhelms, D.E., McCauley, J.F., Trask, N.J., 1987. The geologic history of the Moon. US Geol. Surv. Prof. Pap. 1348.
Wright, J., Rothery, D.A., Balme, M.R., Conway, S.J., 2018. Constructional volcanic edifices on Mercury: candidates and hypotheses of formation. J. Geophys. Res., Planets 123, 952–971.
Zuber, M.T., Smith, D.E., Phillips, R.J., Solomon, S.C., Neumann, G.A., Hauck, S.A., Peale, S.J., Barnouin, O.S., Head, J.W., Johnson, C.L., Lemoine, F.G., Mazarico, E., Sun, X., Torrence, M.H., Freed, A.M., Klimczak, C., Margot, J., Oberst, J., Perry, M.E., McNutt, R.L., Balcerski, J.A., Michel, N., Talpe, M.J., Yang, D., 2012. Topography of the northern hemisphere of Mercury from MESSENGER laser altimetry. Science 80 (336), 217–221.